Tejeda-Serrano, M.; Mon, M.; Ross, B.; Gonell-Gómez, F.; Ferrando-Soria, J.; Corma Canós, A.; Leyva Perez, A.... (2018). Isolated Fe(III)-O Sites Catalyze the Hydrogenation of Acetylene in Ethylene Flows under Front-End Industrial Conditions. Journal of the American Chemical Society. 140(28):8827-8832. https://doi.org/10.1021/jacs.8b04669

Isolated Fe(III)–O Sites Catalyze the Hydrogenation of Acetylene in Ethylene Flows under Front–End Industrial Conditions

María Tejeda–Serrano,[‡,◊] Marta Mon,[†,◊] Bethany Ross,[‡] Francisco Gonell,[‡] Jesús Ferrando–Soria,[†] Avelino Corma,*[,‡] Antonio Leyva–Pérez,*[,‡] Donatella Armentano*[,§] and Emilio Pardo*[,†]

[†]Instituto de Ciencia Molecular (ICMol), Universidad de Valencia, 46980 Paterna, Valencia, Spain

[‡]Instituto de Tecnología Química (UPV–CSIC), Universitat Politècnica de València–Consejo Superior de Investigaciones Científicas, Avda. de los Naranjos s/n, 46022 Valencia, Spain

[§]Dipartimento di Chimica e Tecnologie Chimiche (CTC), Università della Calabria, Rende 87036, Cosenza, Italy

◊These authors equally contributed to the work.

ABSTRACT: The search for simple, earth–abundant, cheap and non–toxic metal catalysts able to perform industrial hydrogenations is a topic of interest, transversal to many catalytic processes. Here, we show that isolated Fe^{III}–O sites on solids are able to dissociate and chemoselectively transfer H_2 to acetylene in an industrial process. For that, a novel, robust and highly crystalline Metal–Organic Framework (MOF), embedding Fe^{III}–OH_2 single–sites within its pores, was prepared in multigram–scale and used as an efficient catalyst for the hydrogenation of 1% acetylene in ethylene streams under front–end conditions. Cutting–edge X–ray crystallography allowed the resolution of the crystal structure and snapshotted the single–atom nature of the catalytic Fe^{III}–O site. Translation of the active site concept to even more robust and inexpensive titania and zirconia supports enabled the industrially relevant hydrogenation of acetylene with similar activity to Pd–catalyzed process.

INTRODUCTION

Nature uses Fe^{II}–containing hydrogenase enzymes to activate and transfer H_2,[1] and following this concept, chemists have designed organometallic Fe^{II} complexes able to catalyze the hydrogenation of unsaturated carbon bonds in organic molecules.[2] More available and robust forms of Fe, such as Fe^{III} oxides, may also dissociate and transfer H_2 to simpler but industrially relevant substrates, i.e. acetylene, if the catalytic site is suitably designed.[3,4] If so, industrial hydrogenations with convenient Fe^{III} solid catalysts could be carried out.

Polyethylene accounts for nearly 30% of the total production of plastics worldwide, which reaches more than 300 million tons every year. Prior to polymerization, the selective hydrogenation of the remnant acetylene (*ca.* 1%) in the raw ethylene stream is necessary, otherwise the polymerization catalyst is poisoned or explosive acetylides can be formed. Traditionally, the hydrogenation of acetylene has been mostly catalyzed by noble metals –including supported noble–metal nanocatalysts– such as Pd, Pt or Ru.[5] Aiming at reducing the ecological footprint associated to the use of such scarce metals in multi–ton industrial processes, further efforts are required to develop novel catalysts based on more abundant and less expensive metals such as transition ones.[6–9]

Metal–organic frameworks (MOFs)[10] –a highly versatile type of crystalline porous materials– have shown excellent results in both gas adsorption[11] and catalysis,[12] which makes them suitable candidates for gas–phase catalysis. MOFs' catalysis can be originated either from open metal sites[13] of the coordination network, or –by taking advantage of the rich host–guest chemistry[14–18] of these porous materials– from active guest species judiciously placed in the pores.[19–23] Indeed, MOFs are especially good for supporting metal cations,[23] complexes[24] or small clusters[19,25] anchoring them to the walls of their channels. As a result, MOFs can exhibit extremely high catalytic activities –often combined with size–selectivity related to such confined state– exceptional characterization of the guest active species –by means of single crystal X–ray diffraction–[26,27] and also improved reuse capabilities compared to metal catalysts in solution.[19]

The preparation of MOFs has been, traditionally, connected with the use of direct self–assembly methods.[28] However, very recently, a new synthetic avenue has emerged for the fabrication of functional MOFs. This is the so–called post–synthetic (PS) methodology,[29–33] consisting firstly on the selection of preformed MOFs and secondly, on the solid–state incorporation[34,35] of the desired functional species within the channels of the MOF.

RESULTS AND DISCUSSION

On this basis, in this work Ni(II) cations hosted in the hydrophilic octagonal pores of a highly crystalline MOF, of formula $Ni_2^{II}\{Ni^{II}_4[Cu^{II}_2(Me_3mpba)_2]_3\} \cdot 54H_2O$ (**1**)[31] [where Me_3mpba^{4-} is the *N,N'*–2,4,6–trimethyl–1,3–phenylenebis(oxamate) ligand (Scheme 1)], were single–

crystal to single–crystal (SC to SC) solid–state PS exchanged by Fe^{III} cations, supported and stabilized within MOF channels by anchoring them to the walls of the net (Figures 1 and S1–S7). This PS exchange yielded the novel compound of formula $[Fe^{III}(H_2O)_6][Fe_2^{III}(\mu\text{–}O)_2(H_2O)_6]_{1/2}\{Ni^{II}_4[Cu^{II}_2(Me_3mpba)_2]_3\} \cdot 72H_2O$ (**2**) (Figure S1).

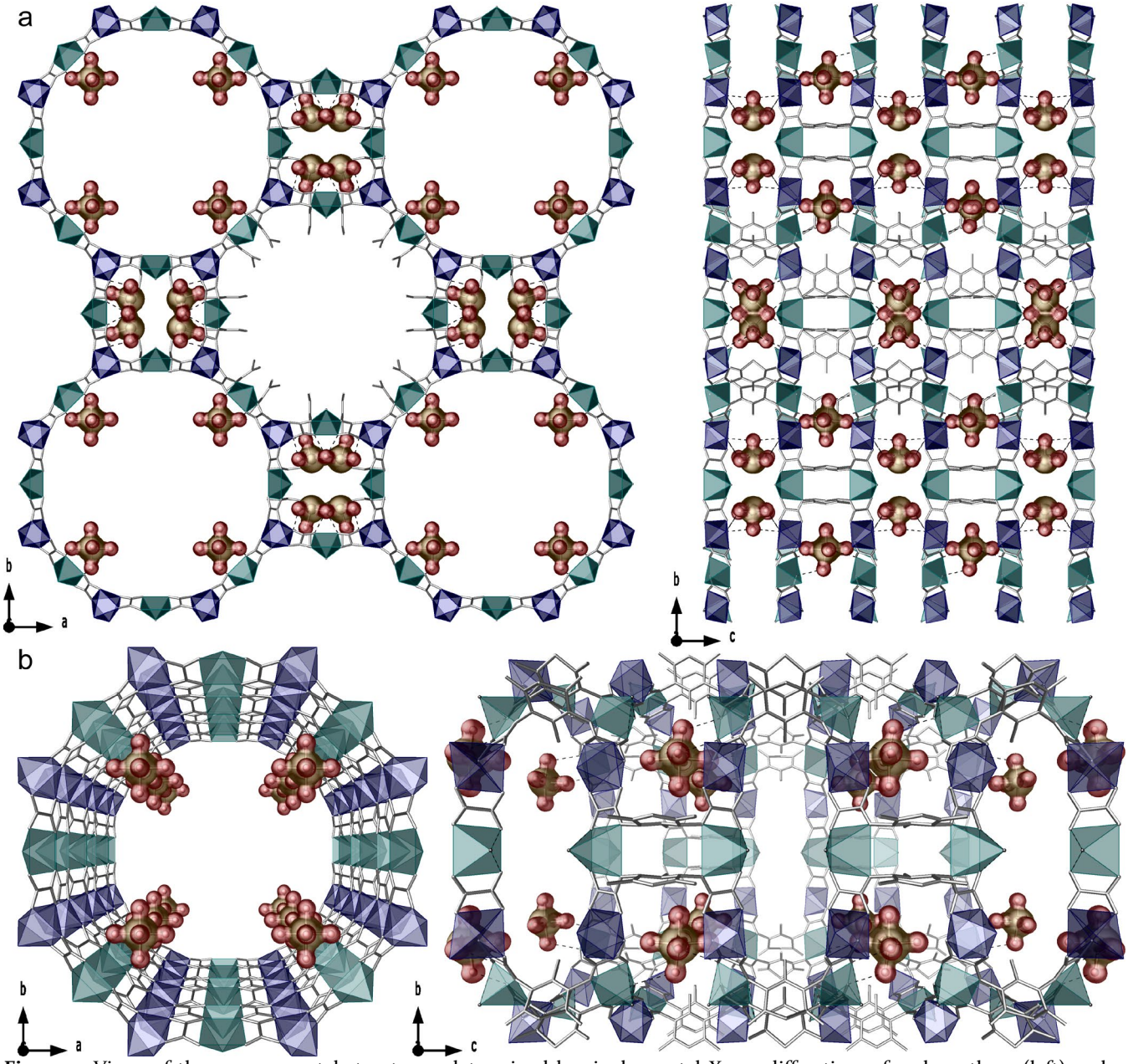

Figure 1. Views of the porous crystal structures, determined by single crystal X–ray diffraction, of **2** along the *c* (left) and *a* (right) axes, respectively. (b) Perspective views of the porous crystal structures of one single channel of **2** along the *c* (left) and *a* (right) axes, respectively. Copper(II) and nickel(II) cations from the coordination network are represented by cyan and blue polyhedra, respectively, whereas the ligands are depicted as gray sticks. Iron(III) cations and water molecules hosted in the channels are represented by gold and red spheres with surface, respectively. Dotted lines represent the hydrogen bonds between the network and the iron units.

The replacement of Ni^{II} cations by Fe^{III} ones, simply soaking crystals of **1** in an aqueous solution of ammonium iron(II) sulfate during one week in open air (see Experimental Section, Supporting Information), was monitored through SEM–EDX and ICP–AES, whereas Fe oxidation state was determined by X–ray photoelectron spectroscopy (XPS, Figure S8a).

After the PS cation exchange, the crystal structure of the new compound **2** unambiguously shows $[Fe^{III}(H_2O)_6]^{3+}$ and $[Fe_2^{III}(\mu\text{–}O)_2(H_2O)_6]^{2+}$ units, confined and retained in the larger accessible hydrophilic octagonal channels and the small hindered square ones, respectively (Figures 1 and S3–S7). Either penta–coordinated Fe^{III} ions from the centrosymmetric dinuclear entities (Figure S4) or the rare hexa–aqua monomers exhibit Fe–O and Fe–OH_2 bond

distances [1.99(1)–2.22(1) Å] in the range of those found in the literature.[36]

The larger accessible void space of the octagonal channels (*ca.* 2.2 nm), contrasting with the very limited accessible space of the smaller ones (Figure 1), suggests that $[Fe^{III}(H_2O)_6]^{3+}$ monomers are prominent catalytic species (*vide infra*). The intrinsic capability of water in *embroidering* infinite H–bonding grids ensures fixation and stabilization of both units in the pores by strong interactions, involving the oxygen atoms of the pore walls from oxamate ligands and water molecules surrounding Fe^{III} ions [$O_{waters}\cdots O_{oxamate}$ 2.89 and 2.85 Å, for monomers and dimers, respectively] (Figures 1, S2, S6 and S7). The highly hydrated and largely accessible MOF's nano–confined space represents a unique and powerful tool to safeguard catalytic species, both stabilizing and triggering them on demand.

The experimental powder X–ray diffraction (PXRD) patterns of a polycrystalline sample of **2** is consistent with the theoretical one (Figure S9a,b) confirming the purity of the bulk. The water content was established by thermogravimetric analysis (TGA, Figure S10) and elemental CHN analyses (Supporting Information). TGA of MOF **2** shows a fast mass loss from room temperature to *ca.* 150 °C. The estimated weight loss value is 32%, which corresponds to the 72 crystallization water molecules hosted in the pores. This abrupt loss in mass is followed by a sort of "plateau" until *ca.* 275 °C with a very smooth mass loss which fits well with the loss of the water molecules coordinated to iron(III) cations. After this "pseudo-plateau", decomposition starts.

Prior to the gas–phase catalysis, the permanent porosity of **2** was confirmed by means of the N_2 and the CO_2 adsorption isotherms at 77 and 273 K, respectively (Figures S11 and S12). N_2 isotherm shows an enhancement of the accessible void space for **2** compared with the ancestor **1**,[31] with a calculated Brunauer–Emmett–Teller (BET) surface area of 1189 m^2/g with a calculated pore size of 1.38 nm. This behavior, showing an increase of a 30% in the maximum amount of N_2 adsorbed compared to the isomorphous compound **1**,[31] suggests an enhanced structural stability after the PS cation metathesis to yield **2**.

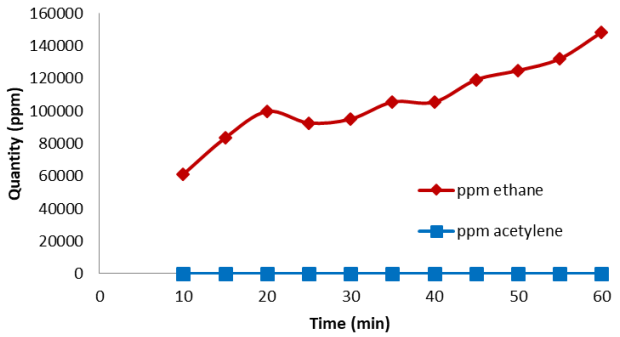

Figure 2. Acetylene (blue squares) and ethane (red rhombuses) amounts in ppm during the continuous hydrogenation of acetylene (1.2%) in an ethylene flow catalyzed by MOF 2 at 150 °C.

Figure 2 shows the hydrogenation of acetylene (1.2%) in an ethylene flow (1 ml/min, 2 bar) catalyzed by MOF **2** (25 mg) in a fixed–bed reactor, with an excess of H_2 (2 ml/min, 4 bar) at 150 °C, and with a gas hourly space velocity (GHSV) of 4000 h^{-1}, which are simulating conditions of real industrial front–end parameters.[37] The results show that acetylene is hydrogenated to less than 10 ppm (instrumental detection limit) and ethane formation is initially below 10%, which are typical values for some Pd industrial catalysts.[38] However, after some time, ethane production steadily increases, which indicates that the MOF catalyst is evolving and losing selectivity under reaction conditions with time. Lower temperatures do not achieve the full hydrogenation of acetylene (Figure S13). In any case, this result represents a step forward on MOFs catalysis. In fact, it is difficult to find in the literature any MOF able to catalyze a continuous process, under simulating industrial conditions.[19,39,40]

XPS measurements of MOF **2** under an H_2 atmosphere within the XPS unit, at 100 ºC (Figure S8, right), show that the original Fe^{III} signal remains unaltered, which supports the stability of Fe^{III} in the MOF when dissociating H_2. Diffuse reflectance ultraviolet–visible (DR UV–vis, Figure S14) measurements confirm the stability of the hexa–aqueous Fe^{III} complex during the hydrogenation reaction,[41] and PXRD pattern after catalysis (Figure S9c) showed that the material remains crystalline with no evidence of nanoparticles (NPs) formation. All these results are in agreement and strongly support both the protecting role of MOF's channels and that the single Fe^{III} site is responsible for the catalysis.

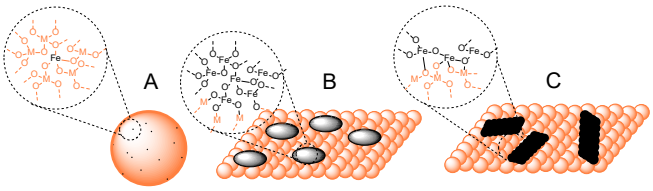

Figure 3. Structures of a) ZrO_2 doped with Fe^{III} atoms, b) ZrO_2 impregnated with Fe^{III} NPs, and c) TiO_2 impregnated with planar Fe^{III} oxide NPs.

To study if single Fe^{III} sites intrinsically dissociate H_2 without acetylene or ethylene participation, isotopic H_2/D_2 exchange experiments under a steady flow of Ar were performed. The results (Figure S15) show the increasing formation of H–D at expenses of H_2 and D_2, when going from 25 to 125 °C, which strongly supports the spontaneous dissociation of H_2 over the catalytic hexa–aqueous Fe^{III} site, under heating conditions. With this data in hand, it seems reasonable that other related aqua–, hydroxo– or oxo–Fe^{III} single sites, such as those in inorganic oxides, may dissociate H_2 and perform the hydrogenation of 1% acetylene in ethylene streams under front–end conditions. Despite MOF **2** is relatively cheap and easy to prepare in large amounts, the study was extended to even cheaper and more robust materials. Figure 3 shows the three different types of inorganic oxo–Fe^{III}

structures prepared, characterized and tested in reaction (see SI, Figures S16–S23, for details).

Structure A consists in isolated Fe^{III} atoms (10 wt%) embedded into a nano–ZrO_2 (≈25 nm) framework (Fe^{III}–$nZrO_2$),[42] with a homogeneous distribution of Fe^{III} atoms along the oxide network, which lefts 0.5 wt% Fe loading on surface, more or less comparable with MOF **2**. Complementary, structure B consists in a 1 wt% of Fe_2O_3 clusters (≈5 nm) supported on nanoZrO_2 (nFe_2O_3–$nZrO_2$), and structure C consists in 0.5 wt% of planar Fe_2O_3 NPs (≈1 nm) supported on nanoTiO_2 (≈25 nm), which maximizes the Fe^{III}–support oxide on surface and, thus, constitutes an intermediate case between isolated oxo–Fe^{III} sites (structure A) and 3D Fe_2O_3 NPs (structure B).[3] For the sake of comparison, commercially–available, isolated Fe_3O_4 NPs were also tested in reaction. For all catalysts, no Fe^0 and only minor amounts of oxo–Fe^{II} were found, together with the major oxo–Fe^{III} species (see SI).

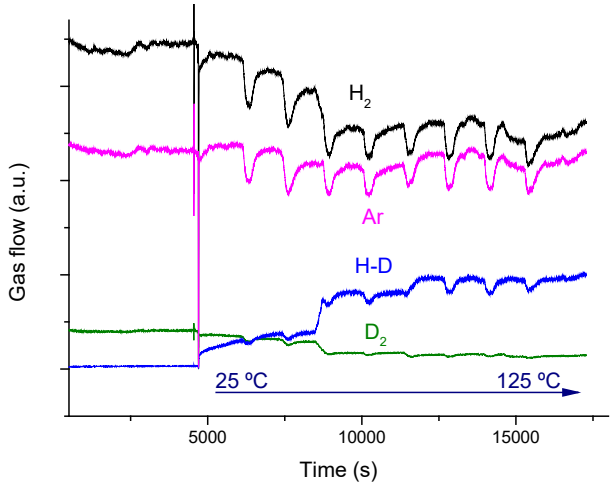

Figure 4. Isotopic H_2/D_2 exchange over Fe^{III}–ZrO_2, with temperature increasing from 25 to 125 ºC after 17500 s (5 h). A constant Ar flow is used as a reference.

Figure 4 shows the isotopic H_2/D_2 exchange experiment for catalyst Fe^{III}–ZrO_2, and formation of H–D can be clearly seen even at 25 °C, with a rapid increase up to 50 °C, and then remaining steady up to 125 °C. Figure 5 shows that, consistent with its lower temperature for H_2 dissociation compared to MOF **2**, Fe^{III}–ZrO_2 catalyzes the hydrogenation of acetylene at just 100 °C and with similar levels of efficiency (<10 ppm acetylene and ethane below 15% during 3 h reaction time). The catalyst works up to 150 °C (Figure S24) with a similar efficiency than at 100 °C, thus providing a reasonable operational window (OW) of temperature to control reaction runaways in industrial conditions. DR UV–vis measurements (Figure S25) confirm the stability of the material at high temperatures. Notice that the operability conditions for Fe^{III}–ZrO_2 are reasonable similar to current Pd–Al_2O_3 industrial catalysts (70–140 °C, ca. 70 °C OW).[38,43,44]

In contrast to Fe^{III}–ZrO_2, isolated Fe_3O_4 NPs do not show any catalytic activity for the hydrogenation of acetylene, and nFe_2O_3–$nZrO_2$ (structure b) only showed a marginal activity at 200 °C (Figure S26). These results illustrate the lack of catalytic activity for Fe_2O_3 NPs, either supported or not.

A new nFe_2O_3–$nZrO_2$ solid with smaller Fe^{III} oxide NPs showed a significant better catalytic activity (Figure S27). Indeed, Fe^{III}–$nZrO_2$ doped with just 1 wt% Fe, thus having in surface 0.05% Fe, works better and at lower temperatures than the nanoparticulated Fe_2O_3 (Figure S28), which strongly supports that isolated Fe^{III}–O sites are catalytically more active than extended Fe^{III}–O– Fe^{III} species. In accordance with this, electronic paramagnetic resonance (EPR) measurements (Figures S29) show that the signals corresponding to isolated Fe^{III} oxide sites (g=4.2, 9.0) increase relatively to Fe^{III} oxide clusters (g=2.0) for 1 wt% Fe–$nZrO_2$,[45] and magnetic susceptibility (Figure S30) confirms these results.[46] It is true that we cannot unambiguously say that all the Fe^{III} sites are free of a second Fe^{III} oxide neighbor, however, the spectroscopic measurements together with the synthesis procedure, which assures a statistical distribution of Fe(III) in the ZrO2 structure, strongly support that isolated Fe(III) oxide are the major catalytic species. 0.5 wt% nFe_2O_3–$nTiO_2$, structure C in Figure 3, shows an intermediate hydrogenating activity between isolated and nanoparticulated oxo–Fe^{III} sites (Figure S31), which is reasonable since the solids present few layers of O–Fe^{III} sites in intimate contact with TiO_2, thus approaching isolated sites in structure A. An 8 hour time experiment (Figure S32) shows that the catalyst is quite robust, keeping a complete acetylene conversion with levels of ethane <10%. Despite having more Fe^{III} on surface, the hydrogenation of acetylene does not proceed further than with MOF **2** or Fe^{III}–ZrO_2, which clearly reflects the importance of having isolated Fe^{III}–O sites for the industrial hydrogenation.

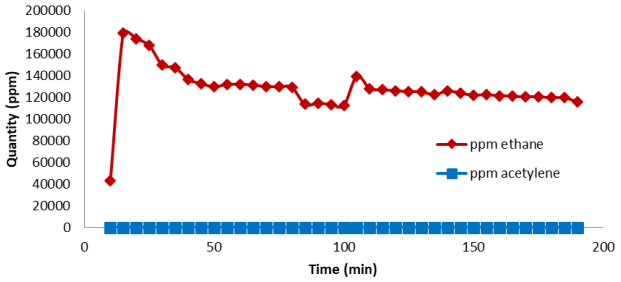

Figure 5. Acetylene and ethane amounts (in ppm) during the continuous hydrogenation of acetylene (1.2%) in an ethylene flow catalyzed by Fe^{III}–ZrO_2 at 100 °C.

Figure 6A shows the result for the hydrogenation in batch of d^2–acetylene,[47] with a rapid exchange of *D* by *H* atoms, up to 43%, while, in contrast, Figure 6B shows that acetylene barely exchanges its protons with D_2 under similar hydrogenation conditions (<1%). These results indicate that the hydroxyl groups, and perhaps also water present on the solid oxide, interact with the alkyne. The kinetic isotopic effect (KIE) calculated for the hydrogenation in batch with H_2 and D_2 is 3.2, in line with previous results with other alkynes.[3] This result confirms that H_2 dissociation intervenes in the rate-determining step of the reaction. Figure 6C shows a proposed mechanism for the

reaction, where H_2 dissociates on the isolated Fe^{III}–O site with the assistance of a hydroxyl group and, then, transferred to acetylene, which coordinates and exchanges *H* atoms with neighboring hydroxyl groups. The adsorption of acetylene (pKa ≈29) on the active sites of the solid through acid–base interactions may explain its higher reactivity respect to ethylene ((pKa ≈50).

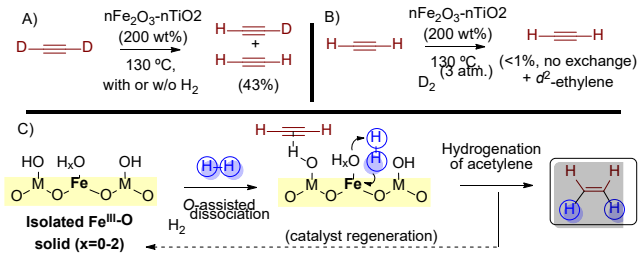

Figure 6. A, B) Isotopic experiments. C) Proposed mechanism for acetylene hydrogenation on isolated Fe^{III}–O catalytic sites.

CONCLUSIONS

In summary, isolated Fe^{III}–O sites on solids catalyze chemoselectively the hydrogenation of acetylene in ethylene streams under simulating front–end industrial conditions. The straightforward preparation of a MOF embedding accessible Fe^{III} sites within its pores, by means of a SC to SC PS cation metathesis, allowed to resolve the structure by single crystal X–ray diffraction, confirming the nature of the Fe^{III} active site. Translation of this Fe active site to more robust and simple metal oxides produced new and cheap, readily available solid catalysts for the industrial reaction, showcasing the cross fertilization between atomically–precise crystalline MOF structures and well–defined supported isolated metal atoms. Beyond mechanistic considerations, the catalysts here presented are just made of relatively non–toxic and inexpensive metals such as Fe, Ti, Cu or Zr, in contrast to the commercial catalysts, which are based on Pd with Ag or Pb additives.[48–50]

EXPERIMENTAL SECTION

Preparation of $[Fe^{III}(H_2O)_6][Fe_2^{III}(\mu\text{–}O)_2(H_2O)_6]_{1/2}\{Ni^{II}_4[Cu^{II}_2(Me_3mpba)_2]_3\} \cdot 72H_2O$ (2): Well-formed hexagonal green prisms of **2**, suitable for X-ray diffraction, were obtained by soaking crystals of **1** (*ca.* 51.8 mg, 0.015 mmol) in an aqueous solution of $(NH_4)_2Fe^{II}(SO_4)_2{\cdot}6H_2O$ (5.8 mg, 0.015 mmol) for 24 hours under aerobic conditions. The process was repeated five more times to ensure the total replacement of nickel atoms hosted in the pores by iron ones. The cation-exchanged crystals (**2**) have the same size and shape as those of the ancestor material (**1**), ruling out a possible dissolution-recrystallization mechanism for this system and strongly suggesting a solid-state process.[51] The crystals were washed with a H_2O/CH_3OH (1:1) solution several times, isolated by filtration on paper and air-dried. Anal.: calcd. for $Cu_6Ni_4Fe_2C_{78}H_{222}N_{12}O_{118}$ (3944.4): C, 23.75; H, 5.67; N, 4.26%. Found: C, 23.61; H, 5.61; N, 4.29%. IR (KBr): ν = 1608 cm^{-1} (C=O).

Aiming at exploring possible industrial applications, a multigram-scale procedure was also carried out. So, a much higher amount of a polycrystalline sample of **1** (4.14 g, 1.2 mmol), was suspended in a H_2O/CH_3OH (1:1) solution of $(NH_4)_2Fe^{II}(SO_4)_2{\cdot}6H_2O$ (0.46 mg, 1.2 mmol) for 12 hours under a mild stirring. The process was repeated 5 times. Finally, the product was collected by filtration, washed with a H_2O/CH_3OH (1:1) solution and air-dried. Anal.: calcd. for $Cu_6Ni_4Fe_2C_{78}H_{222}N_{12}O_{118}$ (3944.4): C, 23.75; H, 5.67; N, 4.26%. Found: C, 23.51; H, 5.65; N, 4.31%. IR (KBr): ν = 1603 cm^{-1} (C=O).

Preparation of Fe^{III}-nZrO_2: The proper amount of $ZrOCl_2{\cdot}8H_2O$ and $FeCl_3{\cdot}6H_2O$ precursors (23.5 mmoles in total) were dissolved in 35 mL of milliQ water, then 27 mmoles of urea were added to the solution. The solution was transferred into one Teflon cup of 100 mL and introduced in a microwave oven. The temperature was increased at 20 ºC/min until 220 ºC, with a dwell time of 10 minutes. Then, the vials were allowed to cool to room temperature and the precipitates were washed and centrifuged several times. The material was dispersed in water and dialyzed until no chloride ions were detected. Finally, water was removed by rotatory evaporation. Following this method, the material obtained is ZrO_2 with the tetragonal structure as the main crystallographic phase with iron introduced in the zirconia structure.

Preparation of nano-ZrO_2: 23.5 mmoles of $ZrOCl_2{\cdot}8H_2O$ were dissolved in 35 mL of milliQ water. The solution was transferred into one Teflon cup of 100 mL and introduced in a microwave oven. The temperature was increased at 20 ºC/min until 220 ºC, with a dwell time of 10 minutes. Then, the vials were allowed to cool to room temperature and the precipitates were washed and centrifuged several times. The material was dispersed in water and dialyzed until no chloride ions were detected. Finally, water was removed by rotatory evaporation. Following this method, the material obtained is ZrO_2 with monoclinic structure.

Preparation of nFe_2O_3-nZrO_2: The metal oxide was wet impregnated at 45ºC with a solution that contained the proper amount of $Fe(acac)_3$ dissolved in 5 mL of acetone. After the impregnation, the materials were dried overnight at 110ºC and calcined with a heating rate of 5 ºC/min at 500 ºC during 2 hours.

Preparation of nFe_2O_3-nTiO_2: 1 g of TiO_2 support was weighed and a solution with the corresponding amount of $FeCl_2$ in 15 ml distilled water was added. The mixture was magnetically stirred at 250 rpm for a few minutes. 50 mg of citric acid was added and the mixture was left to stir for further two minutes. 120 mg of the reducing agent, sodium borohydride ($NaBH_4$), were added under continuous stirring, and the mixture was capped with a rubber septum having a needle piercing, and stirred for 16 h at 250 rpm. After this time, the solid was filtered with a Büchner-Kitasato flask under vacuum. The solution was double-filtered to catch smaller particles, and a dropper was

used to load small quantities of the catalyst solution on to the filter paper. The remaining solid on the filter paper was rinsed with distilled water followed by acetone. The filter paper containing the solid catalyst was carefully transferred into a glass vial and dried for 24 h under vacuum.

Hydrogenations in flow. Typically, 25 mg of solid catalyst (ca. 0.14 cm^3) were placed in a fixed bed tubular reactor, conditioned before each experiment with N_2 gas (see SI for details) and connected to a GC instrument, and ethylene/acetylene (1 %) and H_2 were passed at flowrates and pressures of 2 and 4 ml/min, and 1 and 2 bars, respectively, at temperatures between 70 and 200 ºC.

Hydrogenations in batch. Acetylene (1 bar) and H_2 (3 bars) were charged in a pressure resistant reactor with 10 mg of the desired catalyst, and the mixture placed in a pre-heated oil bath at 150ºC. Gas aliquots were periodically taken and analyzed by GC-MS.

ASSOCIATED CONTENT

Supporting Information Available. Physical techniques. Crystallographic and catalytic details. Figures S1–S32. Tables S1–S2. CCDC reference number: CCDC–1835021. This material is available free of charge via the Internet at http://pubs.acs.org.

AUTHOR INFORMATION

Corresponding Author

* To whom correspondence should be addressed. E–mail: emilio.pardo@uv.es; donatella.armentano@unical.it; anleyva@upv.itq.es; acorma@upv.itq.es.

Notes

The authors declare no competing financial interests.

ACKNOWLEDGMENT

This work was supported by the MINECO (Spain) (Projects CTQ2016–75671–P, CTQ2014–56312–P, CTQ2014–55178–R and Excellence Units "Severo Ochoa" and "Maria de Maeztu" SEV–2016–0683 and MDM–2015–0538) and the Ministero dell'Istruzione, dell'Università e della Ricerca (Italy) (FFABR 2017). M. M. thanks the mineco for a predoctoral contract. Thanks are also extended to the Ramón y Cajal Program (E. P.) and the "Suprograma atracció de talent-contractes postdoctorals de la Universitat de Valencia" (J. F.-S.). A. L.-P. also thanks to fBBVA for the concession of a young investigator grant.

REFERENCES

(1) Lubitz, W.; Ogata, H.; Rüdiger, O.; Reijerse, E. *Chem. Rev.* **2014**, *114* (8), 4081.

(2) Zell, T.; Milstein, D. *Acc. Chem. Res.* **2015**, *48* (7), 1979.

(3) Tejeda-Serrano, M.; Cabrero-Antonino, J. R.; Mainar-Ruiz, V.; López-Haro, M.; Hernández-Garrido, J. C.; Calvino, J. J.; Leyva-Pérez, A.; Corma, A. *ACS Catal.* **2017**, *7* (5), 3721.

(4) Jagadeesh, R. V.; Surkus, A.-E.; Junge, H.; Pohl, M.-M.; Radnik, J.; Rabeah, J.; Huan, H.; Schunemann, V.; Bruckner, A.; Beller, M. *Science* **2013**, *342* (6162), 1073.

(5) Pei, G. X.; Liu, X. Y.; Yang, X.; Zhang, L.; Wang, A.; Li, L.; Wang, H.; Wang, X.; Zhang, T. *ACS Catal.* **2017**, *7* (2), 1491.

(6) Bauer, I.; Knölker, H.-J. *Chem. Rev.* **2015**, *115* (9), 3170.

(7) Albani, D.; Capdevila-Cortada, M.; Vilé, G.; Mitchell, S.; Martin, O.; López, N.; Pérez-Ramírez, J. *Angew. Chemie Int. Ed.* **2017**, *56* (36), 10755.

(8) Liu, L.; Concepción, P.; Corma, A. *J. Catal.* **2016**, *340*, 1.

(9) Sorribes, I.; Liu, L.; Corma, A. *ACS Catal.* **2017**, *7* (4), 2698.

(10) Furukawa, H.; Cordova, K. E.; O'Keeffe, M.; Yaghi, O. M. *Science* **2013**, *341*, 974.

(11) Li, J.-R.; Kuppler, R. J.; Zhou, H.-C. *Chem. Soc. Rev.* **2009**, *38* (5), 1477.

(12) Gascon, J.; Corma, A.; Kapteijn, F.; Llabrés i Xamena, F. X. *ACS Catal.* **2014**, *4* (2), 361.

(13) Valvekens, P.; Vermoortele, F.; De Vos, D. *Catal. Sci. Technol.* **2013**, *3* (6), 1435.

(14) Mon, M.; Lloret, F.; Ferrando-Soria, J.; Martí-Gastaldo, C.; Armentano, D.; Pardo, E. *Angew. Chemie Int. Ed.* **2016**, *55* (37), 11167.

(15) Mon, M.; Ferrando-Soria, J.; Grancha, T.; Fortea-Pérez, F. R.; Gascon, J.; Leyva-Pérez, A.; Armentano, D.; Pardo, E. *J. Am. Chem. Soc.* **2016**, *138* (25), 7864.

(16) Inokuma, Y.; Arai, T.; Fujita, M. *Nat. Chem.* **2010**, *2* (9), 780.

(17) Kitagawa, S.; Matsuda, R. *Coord. Chem. Rev.* **2007**, *251* (21–24), 2490.

(18) Li, P.; Modica, J. A.; Howarth, A. J.; Vargas L., E.; Moghadam, P. Z.; Snurr, R. Q.; Mrksich, M.; Hupp, J. T.; Farha, O. K. *Chem* **2016**, *1* (1), 154.

(19) Fortea-Pérez, F. R.; Mon, M.; Ferrando-Soria, J.; Boronat, M.; Leyva-Pérez, A.; Corma, A.; Herrera, J. M.; Osadchii, D.; Gascon, J.; Armentano, D.; Pardo, E. *Nat. Mater.* **2017**, *16* (7), 760.

(20) Ji, S.; Chen, Y.; Fu, Q.; Chen, Y.; Dong, J.; Chen, W.; Li, Z.; Wang, Y.; Gu, L.; He, W.; Chen, C.; Peng, Q.; Huang, Y.; Duan, X.; Wang, D.; Draxl, C.; Li, Y. *J. Am. Chem. Soc.* **2017**, *139* (29), 9795.

(21) Liu, H.; Chang, L.; Bai, C.; Chen, L.; Luque, R.; Li, Y. *Angew. Chemie Int. Ed.* **2016**, *55* (16), 5019.

(22) Li, B.; Leng, K.; Zhang, Y.; Dynes, J. J.; Wang, J.; Hu, Y.; Ma, D.; Shi, Z.; Zhu, L.; Zhang, D.; Sun, Y.; Chrzanowski, M.; Ma, S. *J. Am. Chem. Soc.* **2015**, *137* (12), 4243.

(23) Genna, D. T.; Wong-Foy, A. G.; Matzger, A. J.; Sanford, M. S. *J. Am. Chem. Soc.* **2013**, *135* (29), 10586.

(24) Abhervé, A.; Grancha, T.; Ferrando-Soria, J.; Clemente-León, M.; Coronado, E.; Waerenborgh, J. C.; Lloret, F.; Pardo, E. *Chem. Commun.* **2016**, *52* (46), 7360.

(25) Mon, M.; Rivero-Crespo, M. A.; Ferrando-Soria, J.; Vidal-Moya, A.; Boronat, M.; Leyva-Pérez, A.; Corma, A.; Hernández-Garrido, J. C.; López-Haro, M.; Calvino, J. J.; Ragazzon, G.; Credi, A.; Armentano, D.; Pardo, E. *Angew. Chemie Int. Ed.* **2018**, *57* (21), 6186.

(26) Mon, M.; Bruno, R.; Ferrando-Soria, J.; Bartella, L.; Di Donna, L.; Talia, M.; Lappano, R.; Maggiolini, M.; Armentano, D.; Pardo, E. *Mater. Horizons* **2018**, doi: 10.1039/C8MH00302E.

(27) Bloch, W. M.; Champness, N. R.; Doonan, C. J. *Angew. Chemie Int. Ed.* **2015**, *54* (44), 12860.

(28) Dul, M.-C.; Pardo, E.; Lescouëzec, R.; Journaux, Y.; Ferrando-Soria, J.; Ruiz-García, R.; Cano, J.; Julve, M.; Lloret, F.; Cangussu, D.; Pereira, C. L. M.; Stumpf, H. O.; Pasán, J.; Ruiz-Pérez, C. *Coord. Chem. Rev.* **2010**, *254* (19–20), 2281.

(29) Evans, J. D.; Sumby, C. J.; Doonan, C. J. *Chem. Soc. Rev.* **2014**, *43* (16), 5933.

(30) Brozek, C. K.; Dincă, M. *Chem. Soc. Rev.* **2014**, *43* (16), 5456.

(31) Grancha, T.; Ferrando-Soria, J.; Zhou, H.-C.; Gascon, J.; Seoane, B.; Pasán, J.; Fabelo, O.; Julve, M.; Pardo, E. *Angew. Chemie Int. Ed.* **2015**, *54* (22), 6521.

(32) Mon, M.; Ferrando-Soria, J.; Verdaguer, M.; Train, C.; Paillard, C.; Dkhil, B.; Versace, C.; Bruno, R.; Armentano, D.; Pardo, E. *J. Am. Chem. Soc.* **2017**, *139* (24), 8098.

(33) Cohen, S. M. *J. Am. Chem. Soc.* **2017**, *139* (8), 2855.

(34) Lin, Z.-J.; Liu, T.-F.; Huang, Y.-B.; Lü, J.; Cao, R. *Chemistry* **2012**, *18* (25), 7896.

(35) Fei, H.; Cahill, J. F.; Prather, K. A; Cohen, S. M. *Inorg. Chem.* **2013**, *52* (7), 4011.

(36) Armentano, D.; De Munno, G.; Mastropietro, T. F.; Julve, M.; Lloret, F. *Chem. Commun.* **2004**, 1160.

(37) Pei, G. X.; Liu, X. Y.; Yang, X.; Zhang, L.; Wang, A.; Li, L.; Wang, H.; Wang, X.; Zhang, T. *ACS Catal.* **2017**, *7* (2), 1491.

(38) Cheung, P. T.-T.; Bergmeister, J.J. III, *WO 03/106020, US patent, Chevron Phillips Chem. Co.,* **2003** and *US0137433,* **2005**.

(39) Pascanu, V.; Hansen, P. R.; Bermejo Gómez, A.; Ayats, C.; Platero-Prats, A. E.; Johansson, M. J.; Pericàs, M. À.; Martín-Matute, B. *ChemSusChem* **2015**, *8* (1), 123.

(40) Zheng, Z.; Xu, H.; Xu, Z.; Ge, J. *Small* **2018**, *14* (5), 1702812.

(41) Chai, L.; Yang, J.; Zhang, N.; Wu, P.-J.; Li, Q.; Wang, Q.; Liu, H.; Yi, H. *Chemosphere* **2017**, *182*, 595.

(42) Gonell, F.; Portehault, D.; Julián-López, B.; Vallé, K.; Sanchez, C.; Corma, A. *Catal. Sci. Technol.* **2016**, *6* (23), 8257.

(43) Armbrüster, M.; Schmidt M.; Kovnir, K.; Friedrich, M.; Weinhold, K.; Grin, J.; Schlögl, R. *WO 09/037301, Max Planck-Gesellschaft zur Förderung der Wissenschaften E. V. patent,* **2009**.

(44) Xu, L.; Spaether, W.; Sun, M.; Boyer, J.; Urbancic, M. *Processing Shale Feedstocks* **2013**, 1.

(45) Jentoft, F. C.; Hahn, A.; Kröhnert, J.; Lorenz, G.; Jentoft, R. E.; Ressler, T.; Wild, U.; Schlögl, R.; Häßner, C.; Köhler, K. *J. Catal.* **2004**, *224* (1), 124.

(46) Ardelean, I.; Peteanu, M.; Filip, S.; Simon, V.; Györffy, G. *Solid State Commun.* **1997**, *102* (4), 341.

(47) Holmsen, M. S. M.; Nova, A.; Balcells, D.; Langseth, E.; Øien-Ødegaard, S.; Heyn, R. H.; Tilset, M.; Laurenczy, G. *ACS Catal.* **2017**, *7* (8), 5023.

(48) Studt, F.; Norskov, J. K.; Christensen, C. H.; Sorensen, R. Z.; Abild-Pedersen, F.; Bligaard, T. *WO 09/086839, Danmarks Tekniske Universitet patent,* **2009**.

(49) Carenco, S.; Leyva-Pérez, A.; Concepción, P.; Boissière, C.; Mézailles, N.; Sanchez, C.; Corma, A. *Nano Today* **2012**, *7*, 21.

(50) Leyva-Pérez, A.; García-García, P.; Corma, A. *Angew. Chem. Int. Ed.* **2014**, *53*, 8687.

(51) Cui, X.; Khlobystov, A. N.; Chen, X.; Marsh, D. H.; Blake, A. J.; Lewis, W.; Champness, N. R.; Roberts, C. J.; Schröder, M. *Chem. Eur. J.* **2009**, *15* (35), 8861.


C_2H_4
Front-End Acetylene Hydrogenation
by MOF-Driven Fe(III) Single Sites
$C_2H_2 + H_2$